J Mater Sci (2010) 45:1567–1578
DOI 10.1007/s10853-009-4125-0

Effect of amount, size, and spatial distribution of intermetallics on incipient localization during plastic deformation

Asim Tewari · Pinaki Biswas

Received: 9 July 2009 / Accepted: 10 December 2009 / Published online: 5 January 2010

Abstract Virtual microstructures having a systematic variation of amount, mean size, standard deviation of size, and spatial arrangement of intermetallics have been synthesized, and their deformation behavior in uniaxial tension has been evaluated using finite element analysis. Four spatial arrangements of intermetallics have been considered in this work, namely: random, clustered, and two-ordered structures. Various mathematical quantities have been developed to quantify the severity of deformation including plastic work density distribution (PWDD), percentile work-density volume criterion (PWC), and percentile stress volume criterion (PSC). This approach eliminates the need for an external trigger in FEA to achieve localization. The method developed has led to a better understanding of the effect of different microstructural attributes on the process of deformation. This has resulted in guidelines for optimizing the microstructure to minimize material damage and thereby maximize ductility.

Introduction

Iron and other transition elements are common impurities in commercial aluminum alloys. These impurities are generally in the range of 0.2–0.3 wt%; lower levels lead to a significant increase in the cost of the aluminum sheet. Since the impurities have a very low solubility in aluminum, they generally precipitate out in the form of dispersed intermetallics that are much harder than the aluminum matrix. The intermetallics have a considerable effect in decreasing the overall ductility and particularly accelerate final fracture [1–5]. A typical microstructure containing such intermetallics is shown in Fig. 1.

The micro-mechanisms of ductile fracture consist of void nucleation, void growth, and final coalescence of the growing voids. Void initiation occurs due to brittle fracture of the intermetallics, or debonding at the particle–matrix interface [6], causing matrix degradation and the material begins to lose its load carrying capability. An independent study on AA5754 aluminum sheets [7] showed that the spatial distribution of the intermetallics has a profound effect on the fracture strain and elongation to failure. Hence, it is reasonable to assume that the distribution, size, and volume fraction of the intermetallics play an important role in the degree of matrix degradation and final failure.

The aim of this work is to study the effect of particle size, its volume fraction, and distribution on deformation severity. The numerical study involves introducing different sizes and distribution of particles into a finite element model. The particles are treated as elastic, whereas the matrix is assumed to be elastic–plastic. In this analysis, no failure model is yet taken, and will be the subject of a future study. The interface is assumed to be perfect, and the particles are assumed not to fail. This limits the applicability of this approach to identify incipient localization before the actual debonding of the particle from the matrix or particle fracture. This is a new approach and will lead to better description of what can be tolerated in the microstructure, since unlike steel, we cannot decrease the amount of intermetallics without using exceptionally expensive aluminum.

Microstructure simulation

Synthetic microstructures were simulated by varying the amount, size, and distribution (spatial pattern) of the second phase particles in a continuous matrix using Monte

A. Tewari (✉) · P. Biswas
General Motors R&D, India Science Lab, Bangalore, India
e-mail: asim.tewari@gm.com

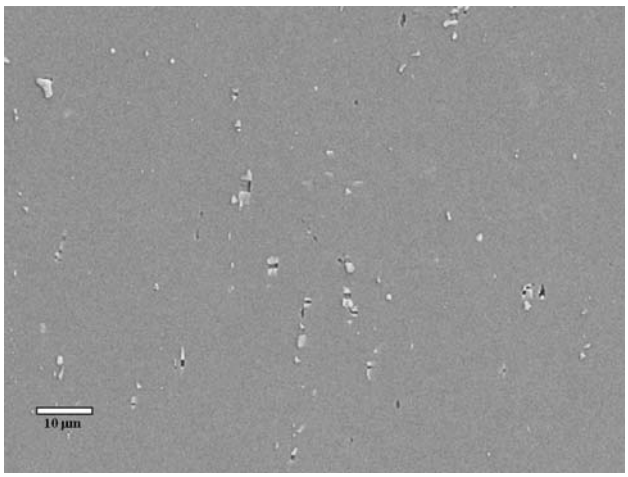

Fig. 1 Typical microstructure of aluminum 6063 showing the Fe-containing intermetallic particles as seen via BSE detector in SEM

Carlo methodology. The choice of amount and size of the particles were based on measured microstructural quantities in rolled sheets of 6063 aluminum alloys. Three different volume fractions of the particles (0.01, 0.02, and 0.03) were simulated. The particles were assumed to be circular with a lognormal size distribution which implies that logarithmic values of the sizes are normally distributed. The different lognormal size distributions chosen, shown in Fig. 2, were such that the desired mean and the standard deviation (SD) of the size (not log of the sizes) are achieved. The mean sizes used in the study are 10, 20, and 30 µm; and the standard deviations are 5, 10, and 15 µm. The spatial occurrences of the particles are varied to produce four different patterns: random dispersion [Random Sequential Addition (RSA)], clustered dispersion, square lattice dispersion, and rotated square lattice dispersion. The choice of these spatial arrangements is inspired by real life examples of random [7], clustered [7], and ordered microstructures [8] seen in commercial materials systems. A total of 100 particles were simulated for each realization of the microstructure. Parts of typical realizations for different spatial arrangements are given in Fig. 3.

Since 100 particles are taken (at random) from the continuous lognormal size distribution, the collection becomes a random set of a stochastic process. Due to the random characteristic, the mean and standard deviation of this set of 100 particles are never exactly equal to the targeted mean and standard deviation of the lognormal distribution. However, this set asymptotically approaches a perfect lognormal distribution when taking the ensemble mean of a large number of these sets. The realization space is chosen as a square of a size such that the mean area fraction of the particles in the square is the desired volume fraction of the particles in the specimen. Since the set of 100 particles is a random set from the continuous

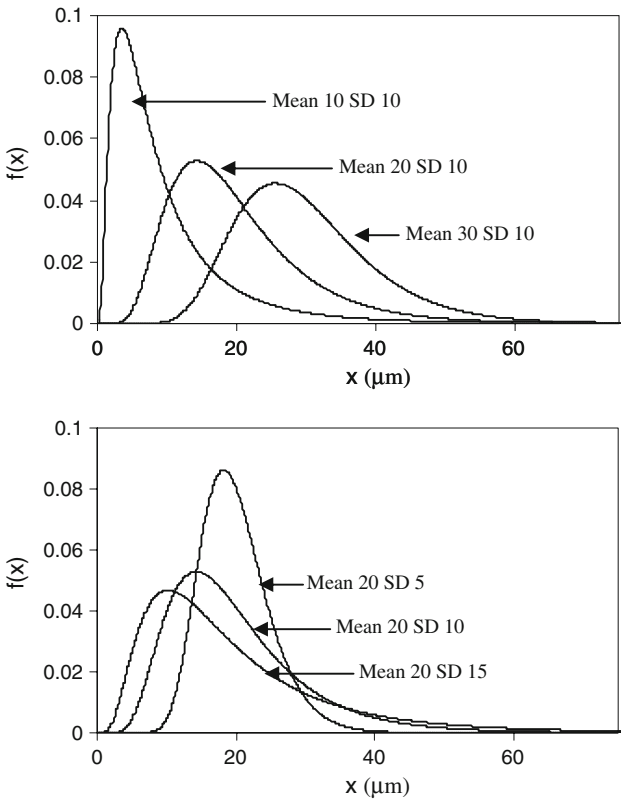

Fig. 2 Different lognormal size distributions (in microns) for the simulation of synthetic microstructure

lognormal distribution, the area fraction of the realizations is also not exactly equal to the targeted value. This is not a shortcoming of the simulation, but a desired characteristic, since we want to exactly mimic the real microstructure, which shows these variations. To eliminate variations from one realization to another, due to stochastic differences in size distribution (and thus area fraction), all realizations for a given mean and standard deviation were performed from the same set of 100 particles. The complete details of all the realizations; their area fractions, mean, and SD, along with their targeted values, are provided in Table 1.

Similarly, on generating random locations of the same set of 100 particles, no two realizations would be exactly the same. This is due to the stochastic character of generating particle locations, which would be seen in RSA and cluster arrangements. To study the variations due to this stochastic process, three RSA realizations are generated for the same 100 particles and compared.

Finite element modeling

The finite element model for the synthetic microstructural analysis has been created using Hypermesh [9]. Since we are dealing with a large number of particles and the process of creating the finite element model for different

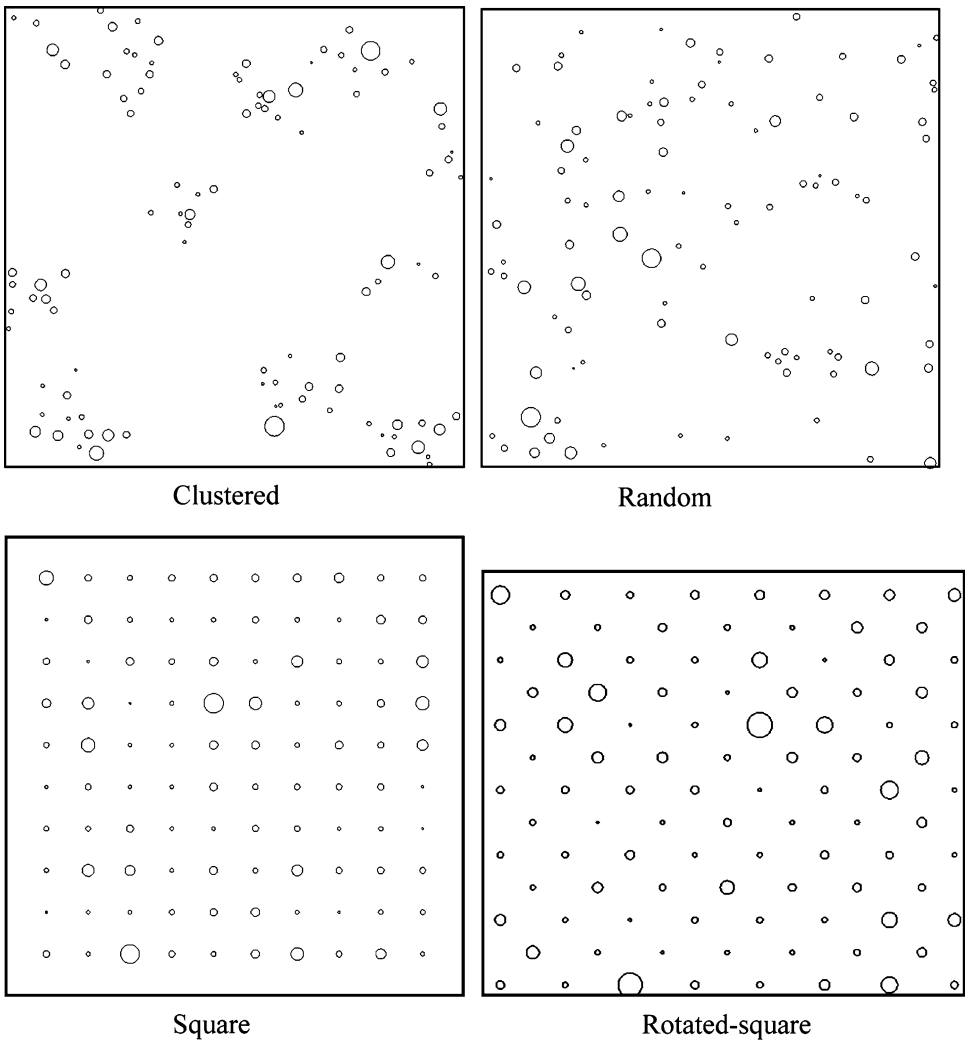

Fig. 3 Different spatial patterns simulated in this study

Table 1 Details of different computer generated microstructural realizations

S. No.	Simulation ID	Volume percent	Mean particle size (μm)	Standard deviation of size (μm)	Spatial arrangement
1	R_2_20_10_1	2	20	10	Random first instance
2	R_2_20_10_2	2	20	10	Random second instance
3	R_2_20_10_3	2	20	10	Random third instance
4	S_2_20_10_1	2	20	10	Square
5	T_2_20_10_1	2	20	10	Rotated-square
6	C_2_20_10_1	2	20	10	Clustered
7	R_1_20_10_1	1	20	10	Random
8	R_3_20_10_1	3	20	10	Random
9	R_2_10_10_1	2	10	10	Random
10	R_2_30_10_1	2	30	10	Random
11	R_2_20_5_1	2	20	5	Random
12	R_2_20_15_1	2	20	15	Random

realizations is repetitive in nature, the entire process of creating the model has been automated through Fortran routines. These routines read the particle information and write sets of command macros for Hypermesh that execute these commands and create the finite element mesh. Another set of Fortran routines reads the node and element information from the mesh file and applies appropriate boundary conditions. Figure 4 shows the finite element

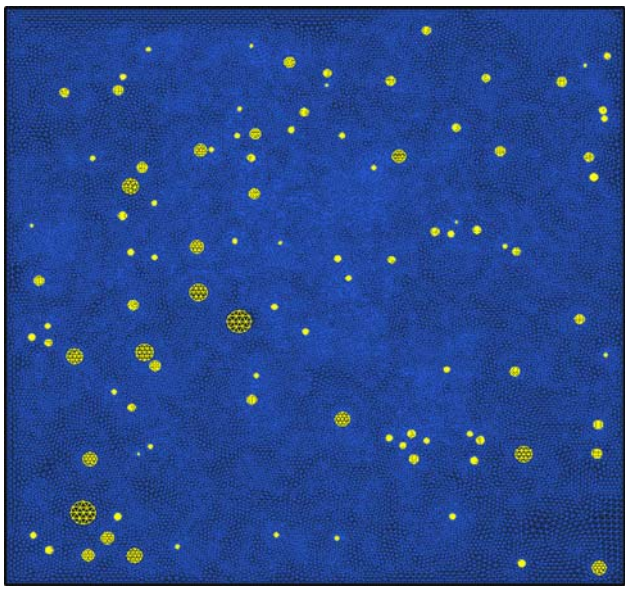

Fig. 4 A typical finite element model for random distribution of 2% volume fraction particles

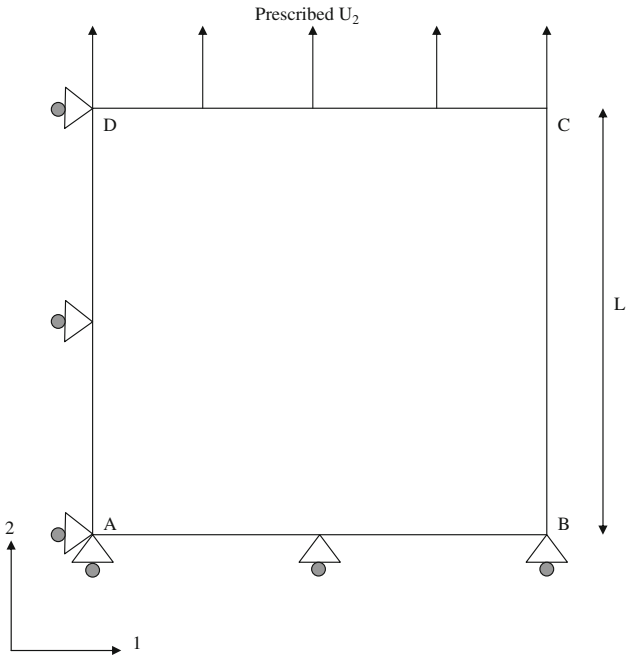

Fig. 5 Schematic of the finite element model with boundary conditions

model of an alloy with 2% volume fraction second phase particles. The particles are distributed randomly with a lognormal size distribution with a mean of 20 μm and a standard deviation of 10 μm.

The schematic diagram of the finite element model and boundary conditions are shown in Fig. 5. The geometry modeled here is a representative volume element (RVE[1]) of the total microstructure. In other words, it is assumed that translational tiling of these RVE's constitutes the whole material. Thus, in order to ensure continuity at the edges, the deformation pattern of the edges of the model has to be identical to that of a neighboring RVE. To enforce this condition, a multi-point constraint (MPC) boundary condition is applied on the edge BC (see Fig. 5), such that it remains straight during deformation. It can be mentioned here that the size of a RVE will depend on the response of interest. In this study, the response of interest is the incipient localization. Simulation results of different realizations, having same mean particle size, standard deviation, and volume fraction, are compared to ensure the sufficiency of the RVE size. In all the cases the loading is uniaxial. The displacement at the edge CD is prescribed to attain a global strain of 40%.

The geometry is modeled using three-noded triangular plane stress elements (CPS3) available in ABAQUS [11]. The implicit finite element solver of ABAQUS was deployed with convergence tolerance parameter for residual force of 5×10^{-3} and criterion for displacement correction of 1×10^{-2}. The matrix material is assumed to obey J_2 flow theory of plasticity [12], whereas, the particles are assumed to be elastic with a Young's modulus $E = 166$ GPa and Poison's ratio, $\nu = 0.3$. The stress–strain response for the elastic–plastic matrix material was represented by the piecewise-linear material hardening model of ABAQUS as shown in Fig. 6. The interface

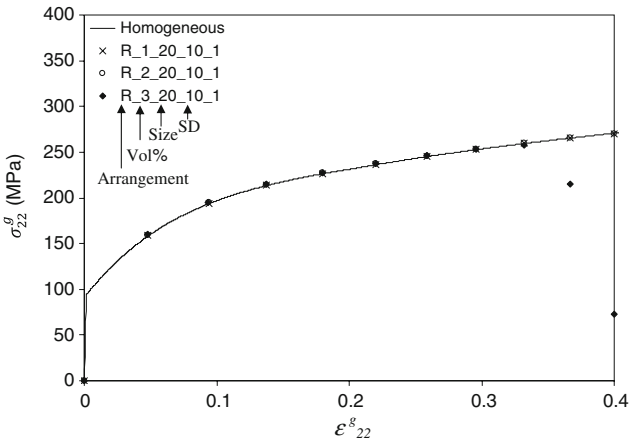

Fig. 6 Comparison of the overall stress–strain response of three random realizations for 1, 2, and 3% volume fraction particles with a monolithic single phase material with no particles (R_1_20_10_a_1 for example means the first instance of a random realization with 1% volume fraction second phase, with mean particle size of 20 μm and SD of 10 μm.)

[1] Representative volume element (RVE) is a statistical concept which implies that a mean property of a large sized sample (equal to or greater than RVE) is statistically equal to the ensemble mean of many smaller realizations [10]. The size of the RVE is given by statistical convergence of the sample mean to the ensemble mean and is characteristic of the microstructure and the property of interest.

Table 2 Different abbreviation and its description

Abbreviation	Description
Homogeneous	Homogeneous
A_V_M_S_X	*A*—Spatial distribution pattern
	R=>Random
	S=>Square
	T=> Rotated-square
	C=>Cluster
	V—Volume fraction of particle in percent
	M—Mean diameter of particle
	S—Standard deviation in particle diameter
	X—Number of Instances of the realization

between the matrix and particles is assumed to be perfect and the particles are assumed not to fail. The aim of the present study is to investigate the effect of particle size, volume fraction, and its distribution on the global deformation of the particle matrix aggregate and on the local deformation of the matrix material.

Different cases considered in this study are tabulated in Table 1 and their abbreviations are shown in Table 2.

Results and discussion

The most common comparison performed in differentiating mechanical properties of materials is their stress–strain response. In light of this view, we compared the global stress–strain response of three simulated Al alloys (two phase aggregates) to the single-phase homogeneous Al matrix material (Fig. 6). The alloy consists of a continuous elastic–plastic Al matrix with a random dispersion of hard second phase particles. All the three cases shown have the same mean particle size (20 μm) and standard deviation (10 μm) but different volume fractions of particles (0.01, 0.02, and 0.03). The global stress is computed on the edge CD in Fig. 5 as

$$\sigma_{22}^{g} = \frac{1}{A}\int_{A} \sigma_{22}\, \mathrm{d}A, \tag{1}$$

where σ_g is the global stress in the current configuration, and A is the current cross-sectional area.

Simulations show that the global stress–strain response of the three aggregates analyzed is similar to the homogeneous material, which is not surprising since the particle–matrix aggregates behave like a composite. But since the particle volume fractions are low, the rule of mixtures would not suggest any significant effect on the stress–strain response. However, for a volume fraction of 3%, localized necking is observed in the matrix beyond 33% strain, and the global stress curve drastically drops beyond this strain

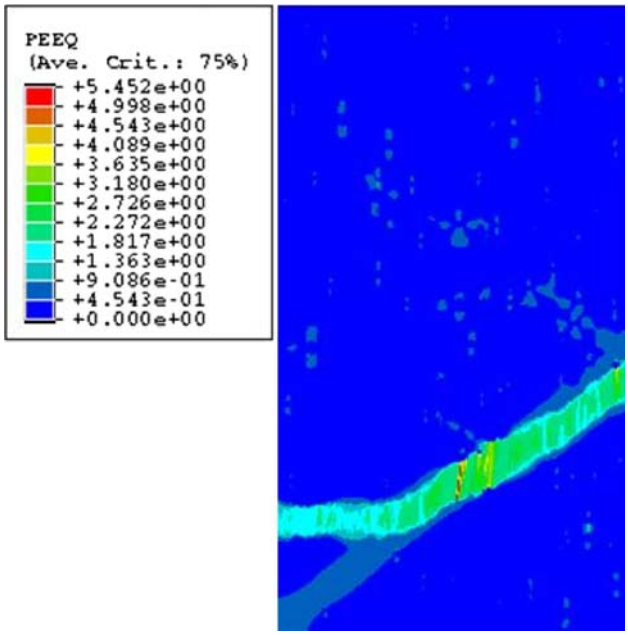

Fig. 7 Contour of equivalent plastic strain for material containing 3% volume fraction particles at a global strain of 0.4. The band of high equivalent strain indicates localized necking

value. It should be noted that no external trigger in the form of inhomogeneity is provided to the model for localization. The localization is self triggered due to the microstructural heterogeneity. The equivalent plastic strain contour for this sample is presented in Fig. 7. The figure shows the band of high equivalent plastic strain where localized necking would take place. Since no failure model is considered in this analysis, the strain level calculated for localized necking would be an overestimate of the true value. In reality, there would be localized damage in the material (in the form of particle fracture, interface debonding and void nucleation), which would cause stress concentrations leading to necking at a lower strain than predicted. It can thus be concluded that the pre-necking global stress–strain response behavior is incapable of differentiating between pure materials and those with low volume fraction of intermetallics.

In order to investigate the effect of particles on local deformation behavior, the probability distribution function, $f(W_d^p)$, of the plastic work density (PWD), W_d^p, for each volume element is investigated. The PWD is given by

$$W_{\mathrm{d}}^{\mathrm{p}} = \int_{0}^{t} \sigma_{ij}\, \dot{\varepsilon}_{ij}^{p} \mathrm{d}t. \tag{2}$$

Here, the repeated index represents summation, and the probability distribution function $f(W_d^p)$ is defined such that $f(W_d^p)\ \mathrm{d}W_d^p$ is the fraction of volume that has a PWD in the range from W_d^p to $W_d^p + \mathrm{d}W_d^p$.

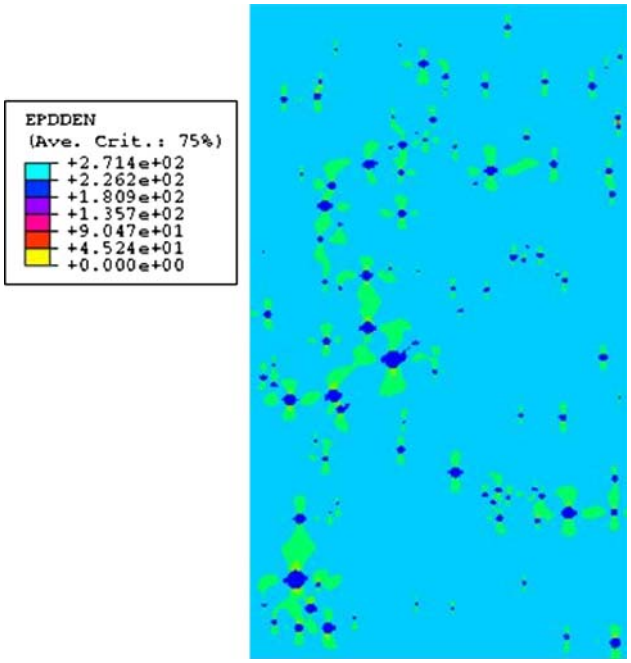

Fig. 8 Contour of PWD at a global strain of 0.366

Close examination of the contours of PWD for the material containing 2 vol% particles at a global strain level of 0.366, Fig. 8, shows that the bulk of the material volume has a PWD ranging between 45 and 90 MJ/m^3, which is within the range for the homogeneous material at this strain. However, there are pockets in the volume where the PWD is much higher. Hence, what could not be captured by global stress–strain response can now be studied by observing the local deformation behavior instead.

To further understand the effect of different microstructural realizations on failure initiation, a new parameter termed as 99.9-percentile work-density volume criterion (99.9 PWC or just PWC in short) is defined as a value of PWD such that at a given global strain, 99.9% of the matrix–particle aggregate volume[2] has a PWD below that level, or in other words 0.1% of the volume has a PWD above that level. This is expressed by the following equation:

$$\left.\begin{aligned} &\int_0^{\mathrm{PWC}} f(W_\mathrm{d}^\mathrm{p})\,\mathrm{d}W_\mathrm{d}^\mathrm{p} = 0.999 \\ &\text{or} \\ &\int_{\mathrm{PWC}}^{\infty} f(W_\mathrm{d}^\mathrm{p})\,\mathrm{d}W_\mathrm{d}^\mathrm{p} = 0.001 \end{aligned}\right\} \tag{3}$$

These equations are essentially a measure of the asymptotic tail of the PWD probability distribution function. Since the failure would not initiate on the average values but at the extremum, this parameter would be strongly correlated to failure initiation. Realizations with a large value of PWC would indicate that there are regions with high plastic deformation indicating possible early failure as compared to realizations with low PWC.

Another mode of failure initiation is through particle fracture. Since the particles are completely elastic, the fracture of particles would be based on a stress criterion. Hence another new parameter, similar to PWC, termed as 99.9-percentile stress volume criterion (PSC) is defined, which is the major principal stress such that at a given global strain, 99.9% of the particle volume has a stress below this value.

Effect of spatial distribution of particles

Plastic work density distribution (PWDD)

The effect of different realizations of random distribution for a given volume fraction of, for example, 2% particles, at different strain levels is shown in Fig. 9. In these three cases, the microstructural realizations were performed with the same 100 particles randomly distributed in the matrix that results in three different instances of random microstructural realizations which have the same volume fraction, same mean, and same standard deviation (S.No. 1, 2, 3 in Table 1). The PWD for a homogeneous material is also plotted in the same figure. It is seen that the PWDD for a homogeneous material is almost a delta function with all the elements having essentially the same amount of plastic work. On the other hand, the material containing 2 vol% particles shows a spread in the PWDD distribution, which increases with an increase in the global strain. This indicates that certain regions of the matrix in the material containing the particles undergo a higher local deformation with a PWD significantly greater than the homogeneous material. One can also observe that at all strains the maximum frequency of PWDD occurs at a higher value of PWD than the homogeneous material. The probability distribution functions of W_d^p for the three different instances having the same random arrangement with the same volume fraction, mean, and SD (S.No. 1, 2, 3 of Table 1) do not show a notable difference, indicating that all instances yield statistically identical results. This implies that the size of the realization is of the order of the RVE for this material. This also means that the probability distribution functions of W_d^p can be used as an indicator to gauge the size of RVE.

Plots of PWDD for square, rotated-square, and clustered spatial arrangements (S.No. 4, 5, 6 in Table 1), Fig. 10, also show similar trends of broadening of the distribution with increasing strain. At all strain levels the rotated-square arrangement of particles shows a narrower band of plastic

[2] It should be noted that since the particles are modeled as completely elastic, the plastic work density would only be present in the matrix.

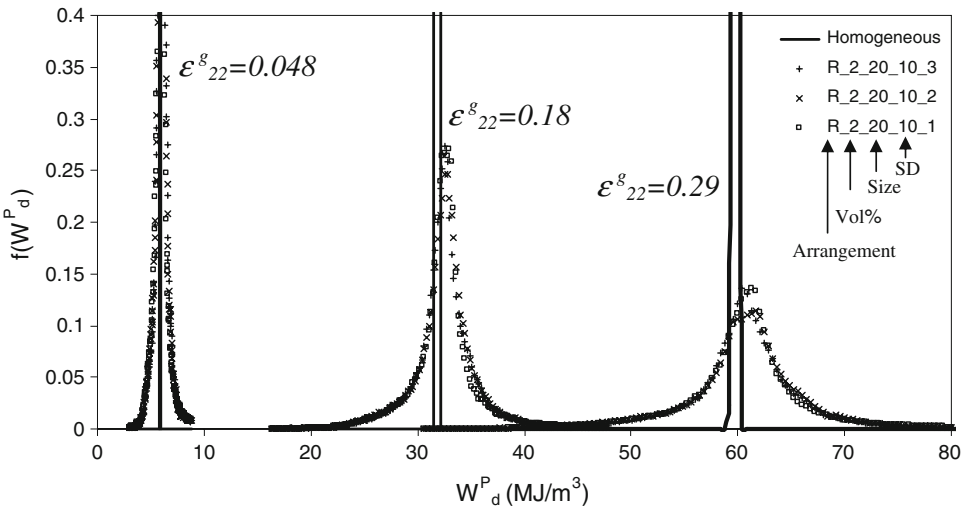

Fig. 9 PWDD for different spatial realizations of particles at three global strains (0.048, 0.18, and 0.29)

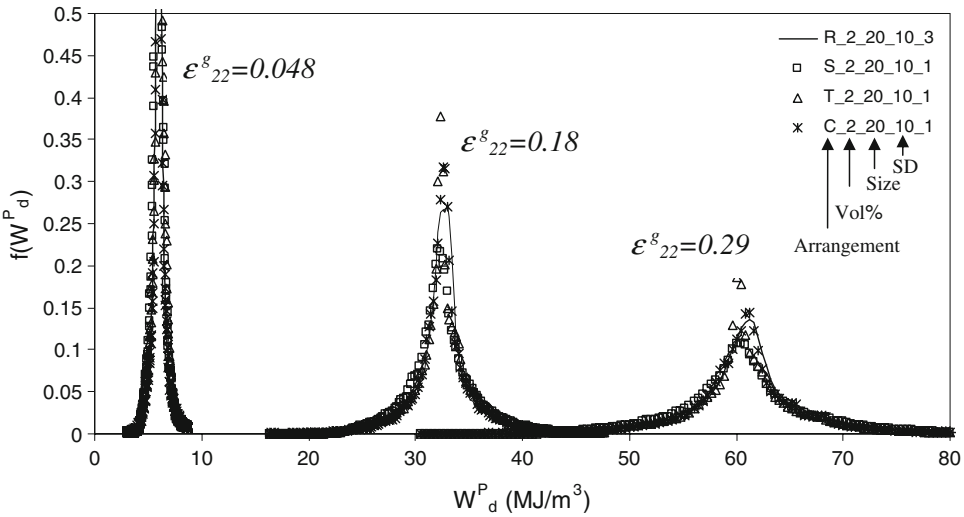

Fig. 10 PWDD for different spatial distribution of particles at three global strains (0.048, 0.18, and 0.29)

work densities, as inferred from a higher peak frequency, indicating that they are closest to the homogeneous material in their PWDD.

Percentile work-density volume criterion (PWC)

The plot of PWDD contains information for all the volume elements, so subtle differences in the tail of the distribution at high values of PWD are not apparent. These differences are captured in the variable PWC. The values of PWC for three different instances of the same random realization (for the same 100 particles, S.No. 1, 2, 3 of Table 1) are plotted in Fig. 11, which shows a pronounced increase in PWC for heterogeneous realizations in comparison to the homogeneous material. This indicates the probability of failure of the matrix at lower strain levels for the material containing the particles.

Similar plots for different spatial arrangements (square, rotated-square, and clustered, i.e., S.No. 1, 4, 5, 6 in Table 1) are given in Fig. 12. It is seen that the PWC values for realizations having random, clustered, and square arrangements are very close and within stochastic variations. On the other hand, the realization containing a

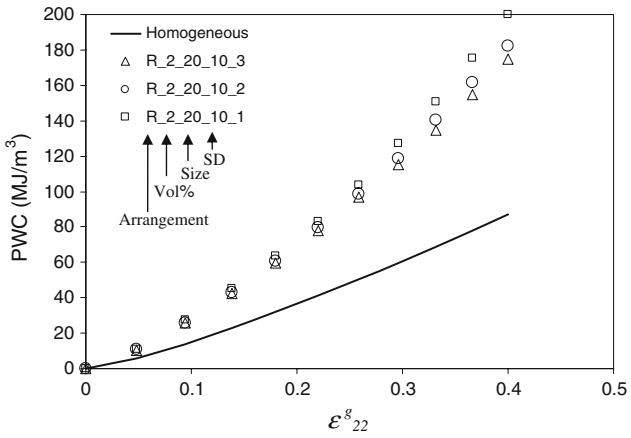

Fig. 11 Plot of 99.9 PWC for different spatial realizations of particles as a function of global strain

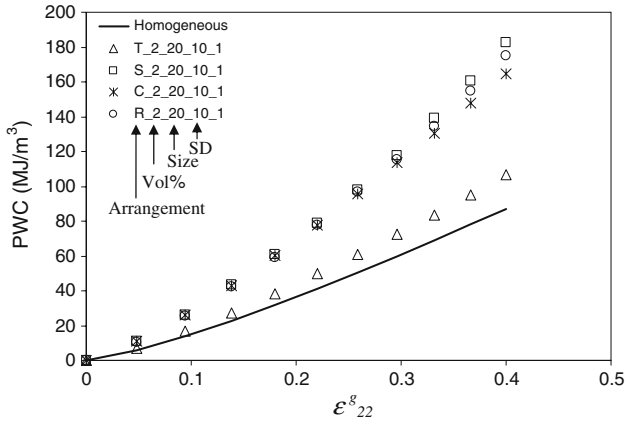

Fig. 12 Effect of spatial arrangement on 99.9 PWC at different global strains

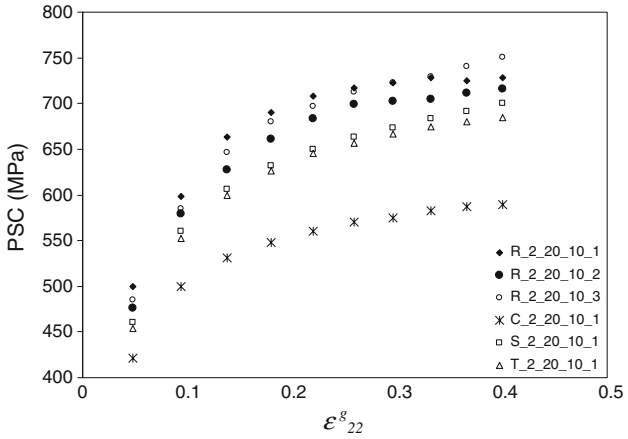

Fig. 13 Plot of 99.9 PSC for particles with different spatial arrangements. The variations in different realizations for the random arrangement are due to the stochastic nature of the microstructure and are expected to occur from region to region in real random materials

rotated-square arrangement of particles has significantly lower values of PWC, which are much closer to the homogeneous material, indicating that this distribution of particles is least damaging to deformation. This distribution is indeed understandable since a rotated-square lattice provides the most open arrangement in two-dimensional space with, on an average, each particle being most distant from each other [13]. The more surprising observation is that the square arrangement (not the rotated-square), in spite of being also an equally open arrangement, shows significantly high values of PWC. Thus, the alignment of the tensile axis with the particle arrangement has a profound effect on the deformation, which is different in the two square lattices.

Percentile stress volume criterion (PSC)

Till now all the analysis was focused on the severity of deformation of the matrix, but equally important is the failure of particles. Since the particles are elastic they would not have any plastic work associated with them and would fail based on some stress criterion. This has led to the 99.9 PSC of the particles. The plots of PSC for different spatial arrangements (S.No. 4, 5, 6 in Table 1) and different realizations (S.No. 1, 2, 3 in Table 1) of random arrangements are given in Fig. 13. Variations for different realizations of random arrangements are seen and attributed to the stochastic nature of the microstructure that occurs in real random materials from region to region. The differences in square and rotated-square realizations are real and cannot be associated with stochastic variations, because these are fixed and unique arrangements, although there could be slight variations due to coupling of particle sizes with the spatial locations. The most interesting and counterintuitive observation is that the PSC in the clustered arrangement is the lowest among all the spatial arrangements. This can be thought of as better load sharing among particles due to a clustered arrangement. However, the PSC values are maximum for random arrangements. This could be due to the presence of isolated particles in this arrangement that may not be sharing the load with any of the other particles.

Thus particles are most likely to fail in a random arrangement and least likely to fail in a clustered arrangement, while from the previous section the matrix is least likely to fail when particles are in a rotated-square arrangement and almost equally likely to fail in all other arrangements.

Effect of volume fraction of particles

Figure 14 displays the PWDD at three global strains for different targeted volume fraction (1, 2, and 3%) of particles arranged randomly (S.No. 1, 7, 8 in Table 1). The difference in PWDD between the three volume fractions increases with increasing global strain. It is clear from the figure that the likelihood of having some regions of the matrix at much higher PWD (W_d^p) is maximum for the structure with 3% volume fraction of particles. This implies that the matrix damage would be most pronounced in the highest volume fraction material.

A comparison of the 99.9 PWC for realizations with different volume fractions together with that for the homogeneous material is plotted in Fig. 15. It can be seen that the PWC is higher for these realizations compared to the homogeneous material, and is greater for higher volume fraction of particles. This indicates that materials with a lower volume fraction of particles have a lower severity of matrix deformation compared to those with a higher volume fraction of particles. The sudden increase of PWC for

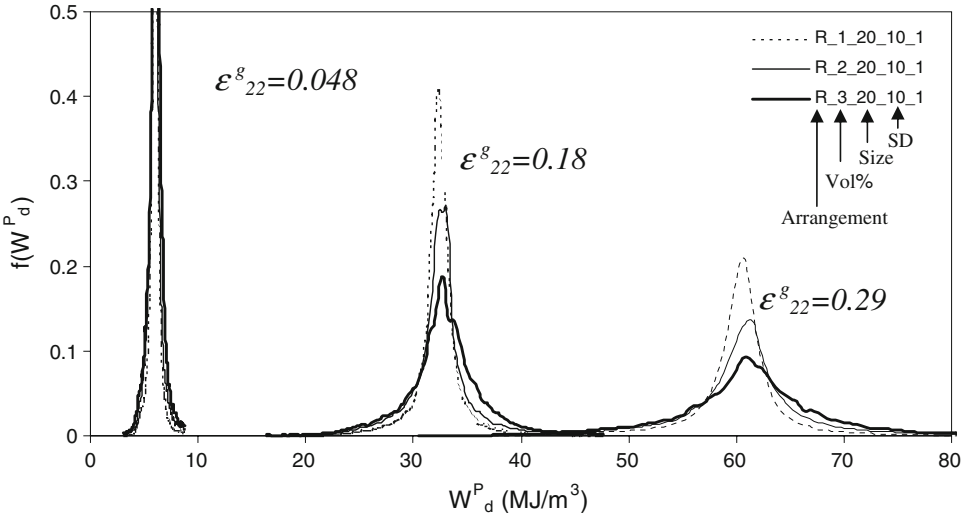

Fig. 14 PWDD for different volume fraction of particles at three global strains (0.048, 0.18, and 0.29)

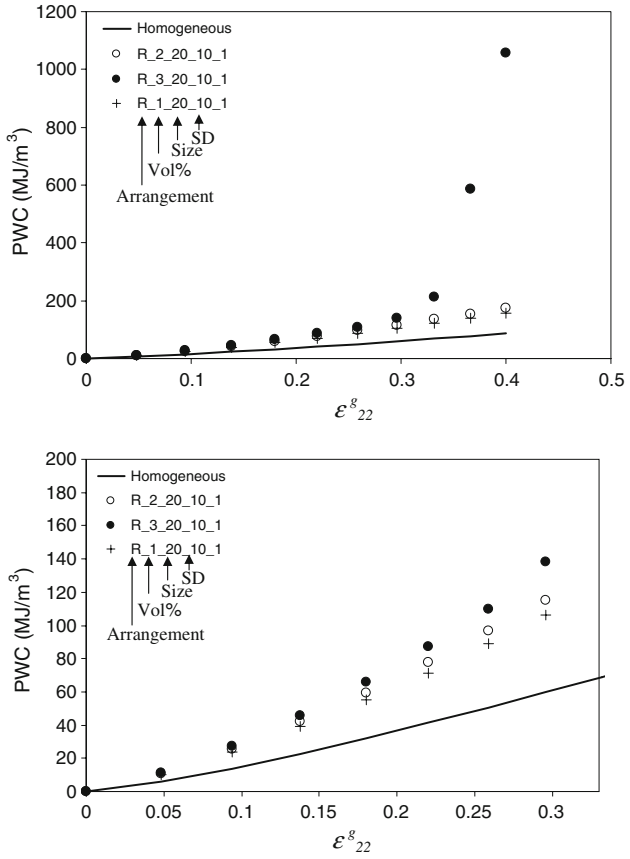

Fig. 15 Variation of 99.9 PWC as a function of global strain for different particle volume fraction

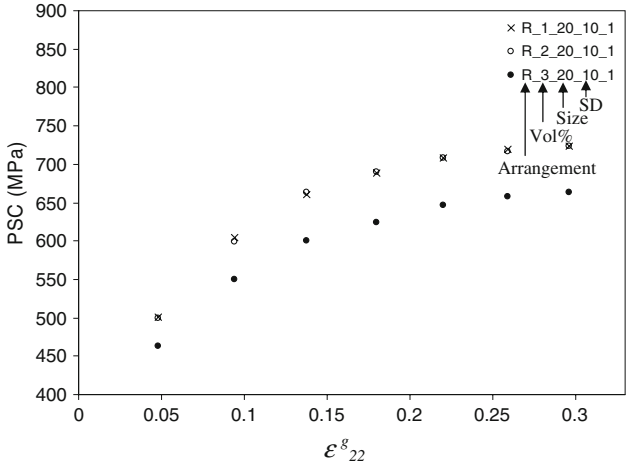

Fig. 16 Variation of 99.9 PSC as a function of global strain for different volume fractions

material with 3% volume fraction of particles, at higher global strains, is due to the formation of a localized neck beyond a global strain of 0.33.

The effect of volume fraction on the stress state of the particles is shown in a plot of PSC versus global strain in Fig. 16. The data for realizations of 1 and 2% volume fraction particles do not differ considerably, however, the PSC for the 3% volume fraction particles is substantially lower. This indicates that it is less likely for particles to fail at higher volume fractions than lower volume fractions. This result is in line with the plots in Fig. 13, where it was concluded that a clustered arrangement would lead to least particle fracture. One can relate the two cases by visualizing the clustered arrangement as a collection of pockets of high volume fraction. The same argument of better load sharing, as used in that section, holds good for these observations. Hence, we see that an increase in particle volume fraction increases the severity of matrix deformation, but decreases the likelihood of particle fracture.

Effect of mean and standard deviation of particle size

Very little distinction in the plots of PWDD for different particle sizes and standard deviation (S.No. 1, 9, 10, 11, 12

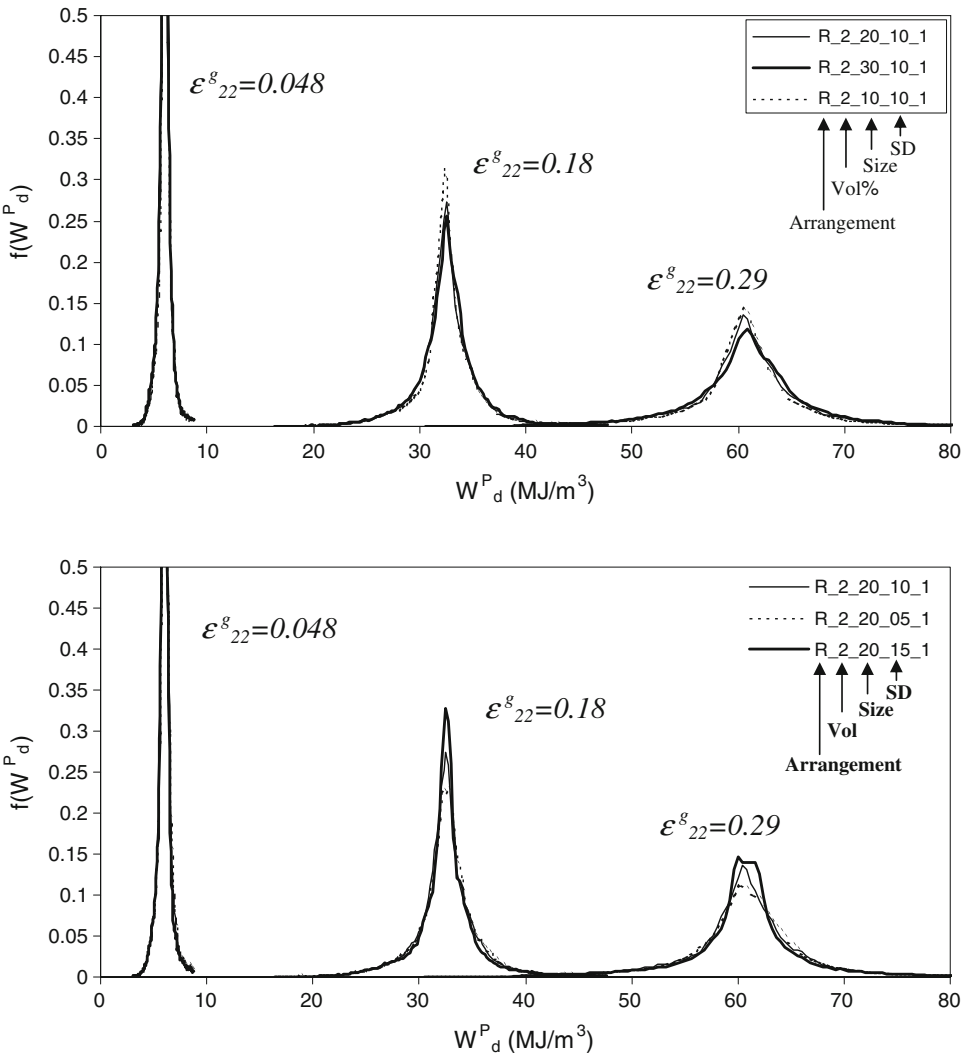

Fig. 17 PWDD for different mean sizes and standard deviation of particles at three global strains (0.048, 0.18, and 0.29)

in Table 1) is observed (Fig. 17). Similarly, very little difference is seen in the 99.9 PWC plots (Fig. 18) for different mean sizes and SDs. The PWC plots for realizations with 10-μm particle size and 15-μm standard deviation are marginally higher than plots with other values of mean and SD. Overall, the differences are very small and the deformation severity of the matrix cannot be strongly correlated with either of the two variables. However, the stress in the particles (as seen in the plot of PSC in Fig. 19) shows a strong correlation with size and SD. It is seen that an increase in mean particle size decreases the PSC, and thus decreases the likelihood of particle fracture (with the assumption that all the particles fail at the same stress and the weakest link theory does not hold). This is counterintuitive, since one would expect just the opposite; however, closer examination of the situation shows that for a constant volume fraction, an increase in particle size would result in a decrease in the total number of particles, which could decrease load transfer to the particles, i.e., less load from the matrix would be shared by the particles, leading to a decrease in PSC. With an increase in particle size, at constant volume fraction, the probability of finding a particle decreases (number of particles per unit area is inversely proportional to the square of particle size). A direct correlation is seen in SD with PSC, which increases with an increase in the SD of the particles. Thus, one can conclude that variations in mean and SD of particle sizes does not have a pronounced effect on the severity of matrix deformation. However, stresses in particles increase with decreasing mean and increasing SD.

It should be noted that this work eliminates the need for the introduction of an unrealistic discontinuity [14–16] in the material for predicting localized necking since it actually brings in inherent microstructural inhomogeneities. An example of this is the realization with 3% volume fraction particles, where necking is predicted due to the presence of hard second phase particles. But since this study does not consider matrix cavitation, particle failure and particle debonding at particle–matrix interfaces, the strains for the onset of localized necking are overestimated.

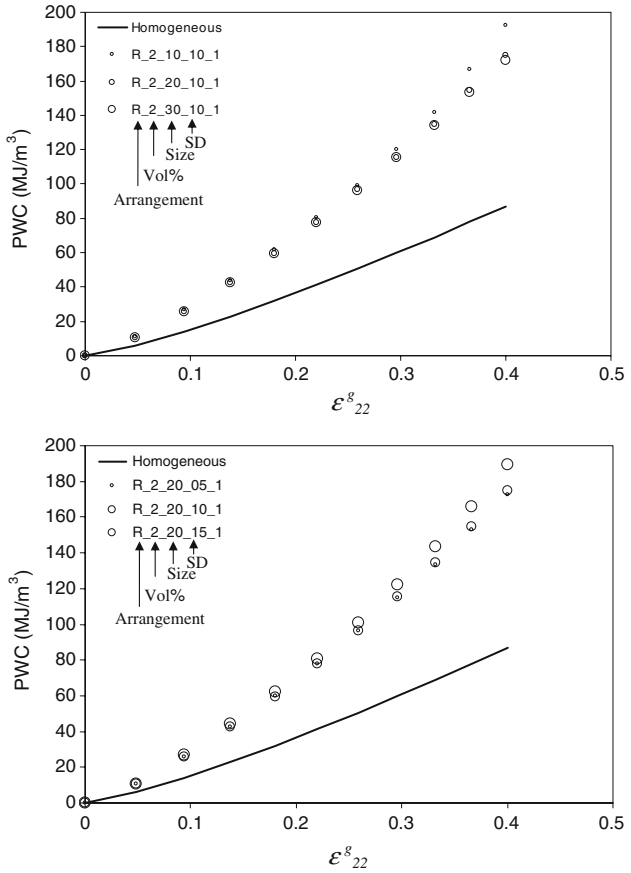

Fig. 18 Plots of effect of mean size and standard deviation on 99.9 PWC. It is seen that the differences are not very large and are within the possible variation due to spatial stochastics

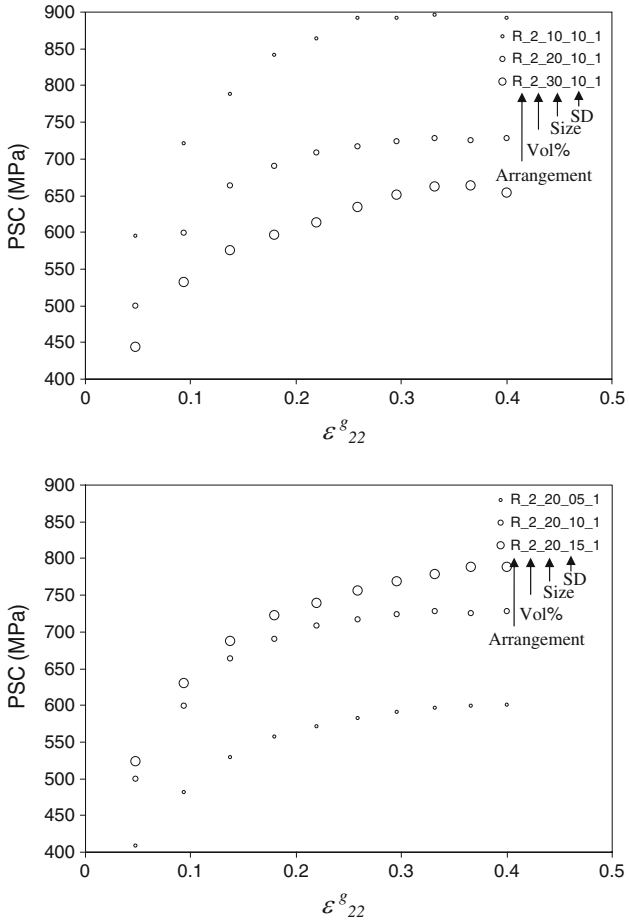

Fig. 19 Plot of variation of 99.9 PSC for different mean sizes and standard deviation of particles

It is seen that the factors that cause an increase in severity of matrix deformation may many times decrease the likelihood of particle fracture. Thus, the optimal microstructure would vary depending on the strength and failure criterion of matrix and particles. A schematic table is given (Table 3) to provide guidelines for determining the optimal microstructure, i.e., with maximum ductility for different matrix and particle properties. Two cases are considered, one with weak matrix and strong interface and particles, and the other with strong matrix and interface with weak particles. A low volume fraction of particles is not always the optimal solution as is seen in the strong matrix interface case. Since in the case of aluminum alloys, the matrix is weaker than the particles, the optimal solution would be in minimizing the volume fraction of particles, provided this does not impact the cost too much.

The inferences drawn from the above analysis should be seen in the light of the assumptions made in this approach. The two principal assumptions of this approach (perfect interface and non-failing particles) are valid only at the onset of localization and not throughout the deformation process. Hence, it would be inappropriate to extend the range of applicability of these results beyond the incipient localization regime. Moreover, another tacit assumption made in this approach is that the matrix is isotropic and homogeneous, whereas the intended application of this approach would be in alloy systems that are polycrystalline [17]. Hence, incipient localization would be triggered not just by second phase particles, but also from any form of inhomogeneity including the discrete individual grains in the polycrystal matrix.

Conclusions

Uniaxial tension simulations using finite element analysis on virtual microstructure was performed. This approach eliminates the need for an external trigger in FEA to achieve localization. The present work has developed the concept of calculating the local PWD, PWDD, PWC, and PSC to understand damage evolution and failure caused by the presence of second phase particles in aluminum sheets.

Table 3 Guidelines for determining the optimal microstructure (i.e., with maximum ductility) for different matrix and particle properties

	Volume %	Particle arrangement	Mean size	Standard deviation
Strong matrix and interface and weak particles	↑	Cluster	↑	↓
Weak matrix and interface and strong particles	↓	Rotated-square	↑*	↓*

* These trends are not very strong and need more investigation

It is concluded that the global stress–strain response behavior is incapable of differentiating pure materials with those having low volume fraction of intermetallics. PWC and PSC are the most sensitive parameters that reflect the influence of intermetallics on formability. The following conclusions emerge that enable us to design microstructures that minimize their effect on plasticity and thus on formability:

1. The presence of intermetallics (on the order of 1–3% volume fraction) does not significantly alter the global load versus displacement curve, but causes large differences in localized plastic-work densities and stresses in the material.
2. The matrix is least likely to fail from a rotated-square arrangement of particles and almost equally likely to fail in all other arrangements as seen by PWC. The particles, on the other hand, are most likely to fail in a random arrangement, which shows the maximum PSC, and least likely to fail in clustered arrangements.
3. An increase in particle volume fraction increases the severity of matrix deformation but decreases the likelihood of particle fracture as seen by PWC and PSC, respectively.
4. Variations in mean and standard deviation (SD) of particle sizes does not have a pronounced effect on the severity of matrix deformation, since PWC is least affected by these changes. However, stresses in the particles increase with decreasing mean and increasing SD as seen by changes in PSC.
5. Results of this work suggest that to maximize formability in the presence of second phase particles, in spite of efforts to reduce their volume fraction, their spatial arrangement should be rotated-square, and they should have a narrow size distribution with larger particle sizes to minimize PWC.

Acknowledgements The authors would like to thank Dr. Raja Mishra and Dr. Anil Sachdev for providing valuable suggestion and editorial comments.

References

1. Nan CW, Clarke DR (1996) Acta Mater 44:3801
2. Wilkinson DS, Maire E, Embury JD (1997) Mater Sci Eng A233:145
3. Babout L, Maire E, Fougeres R (2004) Acta Mater 52:2475
4. Gall K, Horstemeyer M, McDowell DL, Fan J (2000) Mech Mater 32:277
5. Mishnaevsky L, Derrien K, Baptiste D (2004) Compos Sci Technol 64:1805
6. Thomason PF (1990) Ductile fracture of metals. Pergamon Press, Oxford
7. Tewari JM, Tewari A, Tiwari S, Biswas P, Mishra RK (2008) J Microsc 230:192
8. Peng HX, Dunne FPE, Grant PS, Cantor B (2005) Acta Mater 53:617
9. Altair Engineering, Inc. http://www.altair.com
10. Torquato S (2002) Random heterogeneous materials. Springer-Verlag, New York
11. ABAQUS/Standard user's manual, Hibbitt, Karlsson, Sorensen, Inc. http://www.hks.com
12. von Mises R (1913) Göttin Nachr Math Phys 1:582
13. Tewari A, Gokhale AM (2004) Acta Mater 52:5165
14. Marciniak Z, Kuczynski K (1967) Int J Mech Sci 9:609
15. Butuc MC, Gracio JJ, Barata da Rocha A (2003) J Mater Process Technol 142:714
16. Kulkarni A, Biswas P, Narasimhan R, Luo A, Mishra RK, Stoughton TB, Sachdev AK (2004) Int J Mech Sci 46:1727
17. Patil SD, Narasimhan R, Biswas P, Mishra RK (2008) ASME J Eng Mater Technol 130:1